Wang, R. et al. (2013). CNx-modified Fe3O4 as Pt nanoparticle support for the oxygen reduction reaction.
Journal of Solid State Electrochemistry, 17: 1021 – 1028.
http://dx.doi.org/10.1007/s10008-012-1948-4

CNx-modified Fe_3O_4 as Pt nanoparticle support for the oxygen reduction reaction

Rongfang Wang, Jingchun Jia, Hui Wang, Qizhao Wang, Shan Ji and Zhongqun Tian

Abstract

A novel electrocatalyst support material, nitrogendoped carbon (CN_X)-modified Fe_3O_4 (Fe_3O_4-CN_X), was synthesized through carbonizing a polypyrrole-Fe_3O_4 hybridized precursor. Subsequently, Fe_3O_4-CN_X-supported Pt (Pt/Fe_3O_4-CN_X) nanocomposites were prepared by reducing Pt precursor in ethylene glycol solution and evaluated for the oxygen reduction reaction (ORR). The Pt/Fe_3O_4-CN_X catalysts were characterized by X-ray diffraction, Raman spectra, X-ray photoelectron spectroscopy, scanning electron microscopy, and transmission electron microscopy. The electrocatalytic activity and stability of the as-prepared electrocatalysts toward ORR were studied by cyclic voltammetry and steady-state polarization measurements. The results showed that Pt/ Fe_3O_4-CN_X catalysts exhibited superior catalytic performance for ORR to the conventional Pt/C and Pt/C-CN_X catalysts.

Introduction

Among the electrochemical reactions involved in the energy conversion in low-temperature fuel cells, the oxygen reduction reaction (ORR) is the rate-determining process [1]. Platinum is known to possess the best catalytic activity for the ORR among all pure metals when they are deposited on a conductive support material, such as carbon black [2, 3]. Carbon black is commonly used as a support material for Pt-based electrocatalysts, but the corrosion of carbon supports resulting from the electrochemical oxidation in fuel cell operating conditions has been identified to be one of the contributors to the low catalyst performance and durability [4–7].

The ideal support material should have the following characteristics: a high electrical conductivity, easy diffusion of the reactant gas to the electrocatalyst, high enough water absorbent capacity to avoid flooding at the cathode where water is generated, and also showing good corrosion resistance because cathodes are under strongly oxidizing conditions [8]. To enhance the activity of ORR, one of the many strategies is to explore novel materials as catalyst support to host highly active catalysts. Recently, it was found that some oxides, such as SiO_2 [9, 10], Fe_3O_4 [11], and TiO_2 [12], could be used as promising support materials to promote the electrocatalytic stability and even activity of Pt catalysts for ORR. The improved performances depend on the nature of the support. For example, gold particles have a binding energy of about 1.6 eV/defect on an oxygen

vacancy in TiO_2, which determine the dispersion and shape of the gold particles and further result in an improved catalytic activity [13]. Compared with the amorphous carbon support, Suzuki's group found that the metal-oxide support, such as the WO_3 and TiO_2, can suppress the Pt lattice expansion and improve the Pt catalytic activity [14]. Among these oxides, it was found that, in conjunction with Fe_3O_4 and Pt, nanoparticles exhibit high catalytic activity for ORR, showing up to 20-fold increase in mass activity compared with the single component Pt nanoparticles and the commercial 3 nm Pt particles. Unfortunately, Fe_3O_4 is an alkaline oxide with low electrical conductivity and easy to dissolve in acidic condition [11]. Fe_3O_4 is therefore difficult to be used directly as electrocatalysts support at low pH conditions. In order to improve the stability and conductivity of Fe_3O_4, it is necessary to develop an approach to weaken the above-mentioned side effects.

Recently, it has been conclusively shown that forming a good electronically conductive material on the surface of oxides is an effective way to improve the stability and conductivity of oxides [15, 16]. Nitrogen-doped carbon (CN_X) with noble metallic nanoparticles deposited on its surface exhibited an enhanced catalytic activity toward ORR as the CN_X had greater electron mobility and showed n-type or metallic behavior [17–21]. Doping nitrogen into graphite has significant effects on both the morphology and electrocatalytic behavior of Pt nanoparticles [22]. If CN_X can form on the surface of Fe_3O_4, this new material could be a new desirable catalyst support for electrocatalysts, since Pt will exhibit a good durability on the support surface due to anchoring from nitrogen incorporation [23, 24].

In this study, a novel carbon nitride Fe_3O_4 support (Fe_3O_4-CN_X) for Pt electrocatalyst was successfully prepared by carbonizing polypyrrole (PPy, a conducting polymer)-modified Fe_3O_4 (Fe_3O_4-PPy) as shown in the Fig. 1. Subsequently, Pt nanoparticles were deposited on Fe_3O_4-CN_X by a modified organic colloid method in an ethylene glycol (EG) solution. Comparing with commercial Pt/C and Pt/C-CN_X, the Pt/Fe_3O_4-CN_X catalysts exhibited a higher electrocatalytic activity and a better stability for ORR.

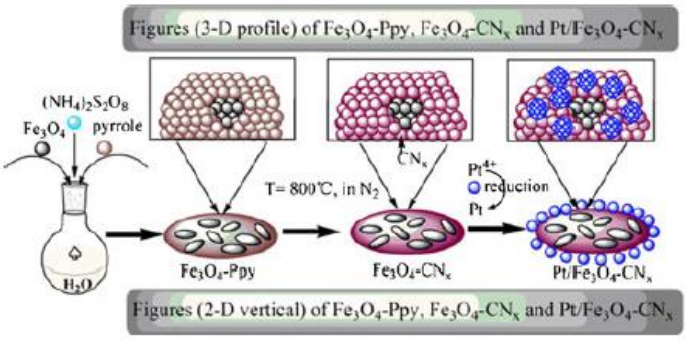

Fig. 1 Scheme of synthesis the new supports and the Pt catalysts

Experimental

Preparation

Fe_3O_4 particles were prepared by the chemical precipitation method. A complete precipitation of Fe_3O_4 was achieved under alkaline conditions. The molar ratio of Fe^{2+}/Fe^{3+} was kept at 1:2 under a nonoxidizing environment. To obtain 1 g of Fe_3O_4 precipitate, 0.86 g of $FeCl_2{\cdot}4H_2O$ and 2.36 g $FeCl_3{\cdot}6H_2O$ were dissolved in 40 ml of deaerated ultrapure water under a N_2 atmosphere while stirring vigorously (1,000 rpm). The solution was heated to 80 °C, and then 5 ml NH_4OH was added. To ensure the complete growth of the nanoparticle crystals, the reaction was carried out at 80 °C for 30 min under stirring conditions. The resulting suspension was allowed to cool down to room temperature and then washed with ultrapure water to remove any unreacted chemicals. Finally, the resulting wet Fe_3O_4 particles were used for the subsequent adsorption procedure. Polymerization of pyrrole on Fe_3O_4 particles (Fe_3O_4-PPy) was carried out in a solution containing $(NH_4)_2S_2O8$ as oxidant. Sixty milliliters of solution containing Fe_3O_4 (0.4 g) and pyrrole monomer (2.0 g) was sonicated at room temperature for 15 min. Eighty milliliters of $(NH_4)_2S_2O8$ solution was slowly introduced into the Fe_3O_4/pyrrole monomer suspension. After that, the suspension was kept at 0 °C under stirring conditions for 6 h and then at room temperature for another 12 h. Subsequently, the solid was filtered and washed with ultrapure water at least three times. The obtained black powder (Fe_3O_4-PPy) was dried at 60 °C for 12 h under vacuum. Preparation of Fe_3O_4-CN_X was carried out via the decomposition of Fe_3O_4-PPy, and the procedure was as follows—1 g of Fe_3O_4-PPy were placed in a quartz tube furnace and then heated to 800 °C with a heating rate of 5 °C min^{-1} under N_2 atmosphere and kept at 800 °C for 2 h. After the furnace cooled down to room temperature, a black powder was obtained. Platinum catalysts (loading ca. 20 wt%) supported on Fe_3O_4-CN_X were prepared by an EG solution method. H_2PtCl_6 (66.4 mg) was dissolved in 30 ml of EG in a flask. The pH of the system was adjusted to 10 by adding 5 wt% of KOH/EG solution. The Fe_3O_4-CN_X (100 mg) black powder was added to the H_2PtCl_6 solution and then heated to 160 °C for 6 h. The resulting catalyst (Pt/Fe_3O_4-CN_X) was filtered, washed with ultrapure water, and dried in a vacuum oven. For comparison purpose, Pt/C-CN_X (20 % Pt, nanoparticles02.5~6 nm) was synthesized using the same procedure, in which carbon was used to replace Fe_3O_4 as support. Pt/C catalyst were purchased from Johnson Matthey (20 % Pt, particles03~6 nm).

Materials characterization

X-ray diffraction (XRD) and X-ray photoelectron spectroscopy (XPS) spectra were generated by using a PHI-5702 multifunctional and a PHI-5702 multifunctional X-ray photo-electron spectrometer (American), respectively. Scanning electron microscope (SEM) images were obtained by using a Hitachi S-2400 (Japan). Transmission electron microscopy (TEM) measurements were carried out using a JEM-2010 electron microscope (Japan) with an acceleration voltage of 200 kV. The chemical composition of the samples was determined using the energy dispersive X-ray analysis (EDX) technique coupled to TEM. The elemental

composition of the Fe_3O_4-CN_X and Pt/Fe_3O_4-CN_X catalysts were evaluated by elemental analysis and EDX. The elemental analysis of carbon (C), nitrogen (N), and sulfur (S) elements were conducted using an organic elemental analyzer (Thermo Flash2000).

Electrochemical characterization

The electrochemical measurements of catalysts were performed on an Autolab electrochemical work station (PGSTAT128N, Eco Chemie, The Netherlands). A conventional three-electrode electrochemical cell was used for the measurements, including a platinum wire as the counter electrode, an Ag/AgCl (KCl 3 M) electrode as the reference electrode and a modified glass carbon electrode (5 mm in diameter, 0.196 cm^2) as the working electrode. All potentials are quoted with respect to the reversible hydrogen electrode (RHE). The thin film electrode was prepared as follows—5 mg of catalyst was dispersed ultrasonically in 1 mL of Nafion/ethanol (0.25 % Nafion). About 8 μL of the dispersion was transferred onto the glassy carbon disc using a pipette and then dried in the air to form catalyst layer on it. Prior to each measurement, the solution was purged with high-purity N_2 (for oxygen-free solutions) or O_2 gas (for oxygen-saturated solutions) for at least 30 min. The Pt-loading on the glass carbon is 40.8 μg_{Pt} cm^{-2}. All the electrochemical tests were carried out at 25 °C.

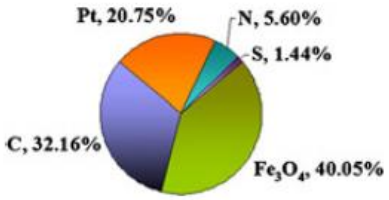

Fig. 2 Contents of Pt/Fe_3O_4-CN_x catalysts

Results and discussion

Properties of catalysts

The composition contents of C, N, S, Fe_3O_4, and Pt are shown in Fig. 2. The figure shows that the Pt loading in the Pt/Fe_3O_4-CN_X catalyst is 20.75 % which is very close to the amount of Pt in the precursors, indicating that the Pt precursor was completely reduced and deposited onto the surface of Fe_3O_4-CN_X catalysts. Since S-containing oxidant ammonium peroxydisulfate was used to prepare Pt/Fe_3O_4-CN_X, small amount of S was also detected in Pt/Fe_3O_4-CN_X catalysts.

Vulcan XC-72R, Fe_3O_4-PPy, and Fe_3O_4-CN_X were investigated by Raman spectroscopy as shown in Fig. 3. From the figure, it can be observed that the peaks of Fe_3O_4-PPy are similar to the results reported by Liu et al. [25]. Figure 3 also shows that the peaks of Fe_3O_4-PPy disappeared after the carbonization step. Here, the positions and intensities of the peaks can provide information about the structure changes occurring on the surface of the catalysts, namely graphite layer defectiveness, resulting from nitrogen doping [26]. In the curves of

Fe_3O_4-CN_X and the Vulcan XC-72R, two peaks are shown around 1,325 and 1,591 cm^{-1}, indicating the presence of the disorder-band (*D*-band) and tangential-mode peak (*G*-band). The *G*-band indicates the presence of crystalline graphite carbon, and the *D*-band is attributed to disorders in the graphite structure. The intensity ratio of I_D/I_G in Fe_3O_4-CN_X curve is ca. 1.15, which is higher than that of the Vulcan XC-72R (0.99). This finding suggests that there are much more defective sites on the CN_X surfaces formed after nitrogen doping [27]. Raman results also indicate that there are more defect sites available on the structure of Fe_3O_4- CN_X XRD patterns of Fe_3O_4, Fe_3O_4-CN_X, and Pt/Fe_3O_4-CN_X are shown in Fig. 4.

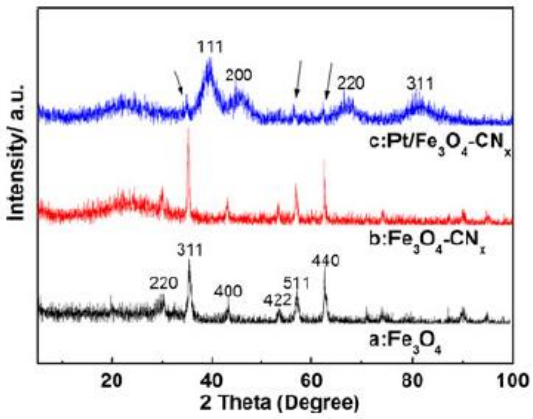

Fig. 4 The XRD patterns of the Fe_3O_4, Fe_3O_4-CN_x, and Pt/Fe_3O_4-CN_x catalysts

Fig. 5 Fe2p XPS spectra of a Fe_3O_4-CN_x and b Pt/Fe_3O_4-CN_x; N1s XPS spectra of b Fe_3O_4-CN_x and d Pt/Fe_3O_4-CN_x; Pt4f XPS spectra of e Fe_3O_4-CN_x and f Pt/Fe_3O_4-CN_x

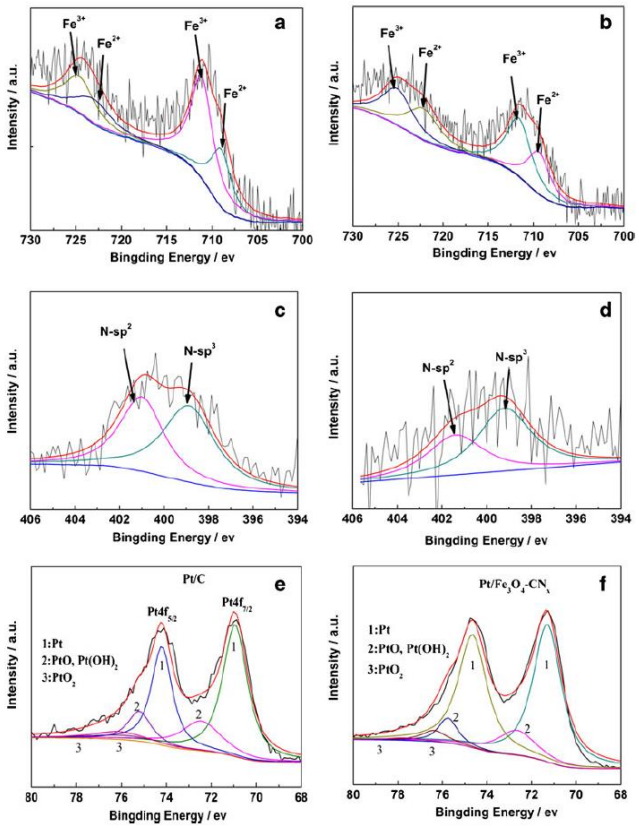

The diffraction peaks of Fe_3O_4 are similar to those found in the literature [28, 29]. A series of characteristic peaks at 30° (2 2 0), 36° (3 1 1), 43° (4 0 0), 53.5° (4 2 2), 57°(5 1 1), and 63° (4 4 0) are well consistent with the data list in JCPDS card no.19-0629. After modification with CN_X, a new broad lump at 2θ025° (Fig. 4b) is found and assigned to the amorphous CN_X, and all other diffraction peaks are similar to these of Fe_3O_4 particles, which imply that the structure of Fe_3O_4 particles does not change after the carbonization step. Besides, the intensities of the peaks of the Fe_3O_4 phase after the carbonization step are a little bit narrower than that prior the carbonization step. This, in turn, may indicate that the thermal treatment induced the growth of the Fe_3O_4 crystallites. After Pt is deposited on the surface of Fe_3O_4-CN_X, the typical diffraction peaks of Fe_3O_4 become relatively small, which may be explained by the relative intensity ration of the Pt, and the Fe_3O_4-CN_X would affect the diffraction peaks. The characteristic peaks of crystalline Pt at 2θ039.7°, 46.3°, 67.6°, 81.4° (JCPDS, no. 04–0802), which are attributed to the (1 1 1), (2 0 0), (2 2 0), and (3 1 1), respectively, are clearly present in the XRD pattern. The XRD results suggest that Pt species were completely reduced to the metallic state by the EG method.

XPS is an efficient method to analyze the surface oxidation states. Figure 5, a and b show the XPS signals of the Fe 2*p*, as well as their spectral deconvolution curves. Two peaks of Fe $2p_1/2$ at 710.3 eV and Fe $2p_3/2$ at 723.9 eV are observed. The absence of the satellite peak at 719 eV, which is a major characteristic of Fe^{3+} in γ-Fe_2O_3 [30], clearly excludes the formation of γ-Fe_2O_3 in the epitaxial layer. The molar ratio of Fe^{2+}/ Fe^{3+} obtained from XPS results is almost 1:2, implying that the iron oxide in the catalyst is Fe_3O_4.

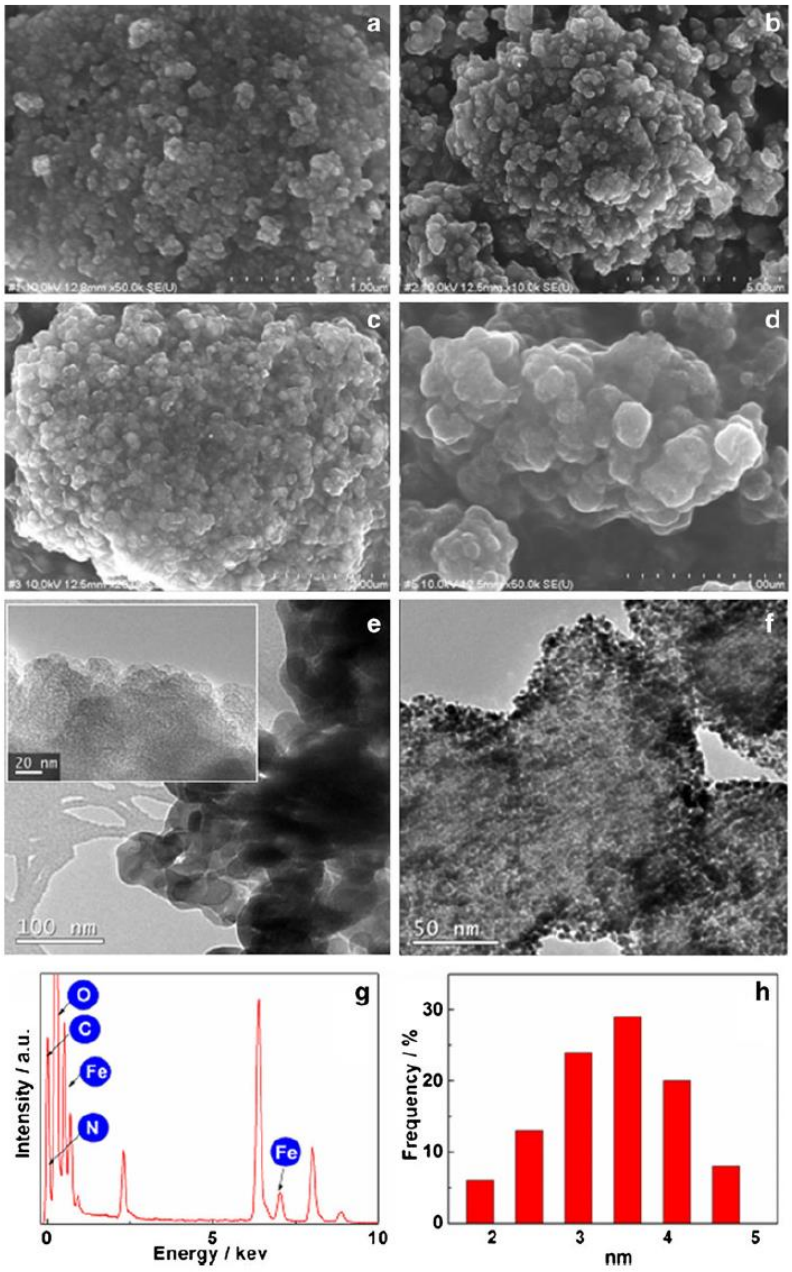

Fig. 6 Scanning electron microscope (SEM) images of Fe_3O_4 (a), Fe_3O_4-PPy (b), Fe_3O_4-CN_x (c), and Pt/Fe_3O_4-CN_x (d); transmission electron microscope (TEM) images of Fe_3O_4-CN_x (e) and Pt/Fe_3O_4-CN_x (f); the *insert* figure of (e) is the edge morphology TEM image of Fe_3O_4-CN_x; EDX spectrum of the Fe_3O_4-CN_x (g); the histograms of particle size distributions of Pt/Fe_3O_4-CN_x (h)

There are four types of nitrogen species in C–N coordination, which are pyridinic (398.6 eV), pyrrolic (400.5 eV), quaternary nitrogen (401.3 eV), and pyridinic N^+–O^-(402– 405 eV). Figure 5 shows that there are two peaks in the N 1*s* spectra for both Fe_3O_4-CN_X and Pt/Fe_3O_4-CN_X catalysts.

The peak at high-binding-energy, i.e., 401.2 eV, corresponds to nitrogen bonded in a threefold coordination (N-sp^2), which is a feature of N bonding with the graphite layer. The other peak present in the low-binding-energy side corresponds to the pyridine-type N bonding (N-sp^3), which results from the interlinked node morphology inside the CN_X [31]. The area of the XPS peak could be qualitatively estimated the level of element content. Comparing Fig. 5, c and d, the integrated area ratio of N-sp^2 decreased after Pt

nanoparticles were deposited onto the surface, which imply that the amount of N bonded with graphite layer (N-sp^2) was decreased after Pt nanoparticles were deposited on the surface.

Figure 5, e and f depict Pt 4*f* binding energy region of Pt/C and Pt/Fe_3O_4-CN_X catalysts. Two peaks are observed at (71.0, 74.2 eV) for Pt/C and (71.4, 74.8 eV) for Pt/Fe_3O_4-CN_X, which are attributed to $4f_{7/2}$ and $4f_{5/2}$ of metallic Pt, respectively. Compared with the XPS of Pt/C, there is a clear shift of the Pt 4*f* peak in the XPS of the binding energy of Pt/Fe_3O_4-CN_X, shifting to higher energy region, which result from the stronger interaction between Pt and support and forming electron-rich Pt [32]. To identify the surface oxidation states of Pt, the Pt 4*f* spectrum were deconvoluted into three doublets which correspond to the different oxidation states of Pt. These three pairs of peaks indicate that there are three different oxidation states present in the Pt/C and Pt/ Fe_3O_4-CN_X catalysts. The amount of Pt species is related to the relative intensities of these three peaks. The highest doublet at around 71 and 74 eV is attributed to metallic Pt, which show that the dominant Pt species in the catalysts is metallic Pt.

Figure 6 show SEM images of Fe_3O_4, Fe_3O_4-PPy, Fe_3O_4- CN_X, and Pt/Fe_3O_4-CN_X. It can be observed that Fe_3O_4 particles are aggregated with each other in Fig. 6a. After Fe_3O_4 particles were modified by PPy, a coral-shaped morphology was formed (Fig. 6b). Fe_3O_4-CN_X shown Fig. 6c in also clearly shows a coral-shaped with a quite rough surface after the carbonization step. Figure 6e shows a TEM image of Fe_3O_4-CN_X. Here, it was found that the radius of single coral-like Fe_3O_4-CN_X particle is in the range from 30 to 60 nm. The inserted figure in Fig. 6e represents the edge morphology of Fe_3O_4-CN_X and clearly shows that a rough surface was formed on the Fe_3O_4-CN_X particles, allowing more available sites for immobilizing Pt nanoparticles. The EDX spectrum (as shown in Fig. 6g) indicates that there are C, N, O, and Fe elements present in Fe_3O_4-CN_X. Figure 6, d and f show typical SEM and TEM images of Pt/Fe_3O_4-CN_X catalyst, respectively. It was observed that the Pt nanoparticles were well dispersed on the surface of Fe_3O_4-CN_X support. The diameters of Pt nanoparticles range from 2 to 5 nm which were obtained by measuring 300 particles from Fig. 6f, and the average diameter is 3.6 nm.

Electrochemical characterizations

Figure 7 shows the electrochemical characterizations of the Fe_3O_4-CN_X samples. The cyclic voltammetry (CV) in Fig. 7a shows an oxidation peak (O_1) at ~0.62 V versus RHE in the scan toward positive potential and a reduction peak (R_1) at ~0.50 versus RHE in the negative scan. Both peaks may be related to the overlapped peaks of quinone/ hydroquinone peaks and the same Fe(III)/Fe(II) redox system [33]. The stability of the Fe_3O_4-CN_X sample was evaluated by repeated CVs with the appropriate lower and upper potential limits in N_2-purged 0.5 M H_2SO_4 solution at room temperature. The CVs shown in Fig. 7b did not change after 1,500 cycles, indicating that the Fe_3O_4 nanoparticles were

covered by CN_X Figure 8a shows the cyclic voltammograms of Pt/Fe_3O_4-CN_X, Pt/C-CN_X, and Pt/C catalysts in deaerated 0.5 M H_2SO_4 at a scan rate of 50 mVs^{-1}.

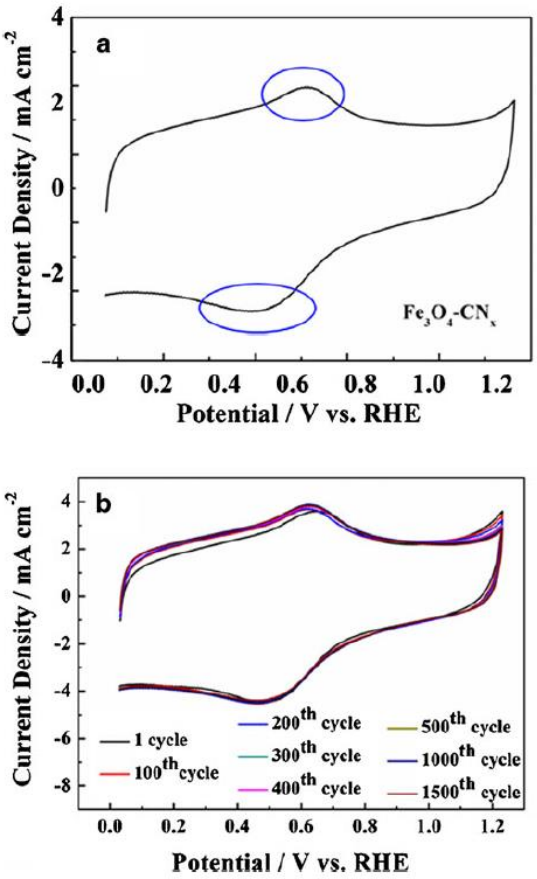

Fig. 7 a CV cycles of the Fe3O4-CNx sample in N2-purged 0.5 M H2SO4 solution at room temperature (sweep rate 50 mV s-1), and b stability of the Fe3O4-CNx sample in N2-purged 0.5 M H2SO4 solution at room temperature (sweep rate 100 mV s-1). In addition, there are some inappropriate expression.

The characteristic peaks in the region (from 0 to 0.3 V versus RHE) are attributed to atomic hydrogen adsorption and desorption on the Pt nanoparticle surfaces. The oxidation and reduction peaks in the curve of Pt/Fe_3O_4-CN_X should be in a similar manner with respect to the curve of Fe_3O_4-CN_X. The change in the reduction peak is due to the quinone/hydroquinone peaks, and the same Fe(III)/Fe(II) reduction peak overlapped with the peak of the Pt oxide reduction. The electrochemical active surface area (*ECSA*) provides important information regarding the number of available active sites on the catalyst. The *ECSA* includes not only the catalyst surface available for charge transfer but also the access of a conductive path to transfer the electrons to and from the electrode surface [34]. The *ECSA* for the catalysts could be estimated from the integrated charge of the hydrogen adsorption/desorption region of the CV. The areas in square meters per gram are calculated from the following formula assuming a correlation value of 0.21 $mCcm^{-2}$ and Pt loading [35]:

$$ECSAs\left(\mathrm{m^2 g_{Pt}^{-1}}\right) = Q_{\mathrm{H}}/(0.21 \times W_{\mathrm{Pt}}) \qquad (1)$$

where *ECSAs* is tQ_{H} is the amount of charge exchanged during the adsorption of hydrogen atoms on Pt deducted the charge of double layer, W_{Pt} is the Pt loading on the electrode. The *ECSAs* calculated from the hydrogen adsorption peaks are 14.3, 17.1, and −1 12.9 $\mathrm{m^2}$ $\mathrm{g_{Pt}}$ for Pt/Fe_3O_4-CN_X, Pt/C-CN_X, and Pt/C catalysts, respectively. The *ECSA* value of Pt/Fe_3O_4-CN_X was found to be 11 % higher than that of conventional Pt/C, indicating that Pt nanoparticles on the Fe_3O_4-CN_X have more electrocatalytic active sites than conventional Pt/C.

Figure 8b shows the linear sweep voltammograms, scanned in the negative-going scan, of Pt/C, Pt/C-CN_X, and Pt/Fe_3O_4- CN_X for ORR. In the Tafel region and the mixed potential region, it was found that the ORR currents of Pt/Fe_3O_4-CN_X and Pt/C-CN_X start to increase at about much higher potentials which are more positive than that of Pt/C, indicating the activity of Pt nanoparticles on the Fe_3O_4-CN_X and C-CN_X supports are higher than that of conventional carbon support. The half-wave potentials of Pt/Fe_3O_4-CN_X, Pt/C, and Pt/C-CN_X are 0.83, 0.81, and 0.82 V versus RHE, respectively, which demonstrate that the catalytic activity of Pt/Fe_3O_4-CN_X catalysts toward the ORR is higher than that of Pt/C and Pt/C-CN_X. The higher activity in electrochemical performance may be related to the following two factors: (1) The Pt/Fe_3O_4-CN_X presented the highest electrochemical surface area, so it is expected to observe an enhanced current in comparison to the Pt/C; (2) the electronic properties are also enhanced due to an extra electron from the doping nitrogen atoms.

The degradation of an electrocatalyst can be evaluated by repeated CVs with the appropriate lower and upper potential limits in an acid solution [36]. The CVs for Pt/C and Pt/ Fe_3O_4-CN_X show a significant decrease in platinum *ECSA* for Pt/C but little for Pt/Fe_3O_4-CN_X as the number of cycles increases, which are shown in Fig. 8c.

Here, the kinetic currents (i_k) were always calculated from the ORR polarization curve by mass-transport correction and normalized to the mass activity of the different catalysts [37], and the mass activity of the different catalysts were shown in the Fig. 8d. Prior to 500 cycles, the Pt/Fe_3O_4-CN_X exhibits a mass activity of 201.8 mA $\mathrm{mg^{-1}Pt}$ at 0.80 V (versus RHE) and 80.9 $\mathrm{mAmg^{-1}Pt}$ at 0.85 V versus RHE, which is 1.4 and 1.7 times greater than the value obtained for the Pt/C catalyst, i.e., 147.8 mA $\mathrm{mg^{-1}Pt}$ at 0.80 V versus RHE and 48.0 $\mathrm{mAmg^{-1}Pt}$ at 0.85 V versus RHE.

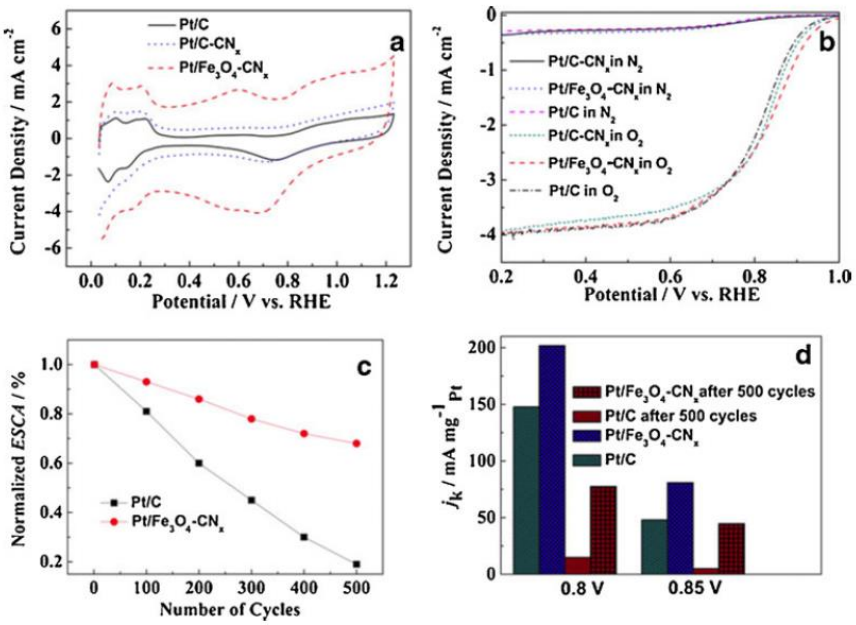

Fig. 8 **a** CV cycles of the Pt/Fe_3O_4-CN_x, Pt/C-CN_x, and Pt/C catalysts in N_2-purged 0.5 M H_2SO_4 solution at room temperature (sweep rate, 50 mV s^{-1}). **b** ORR polarization curves of the Pt/Fe_3O_4-CN_x, Pt/C-CN_x, and Pt/C catalysts in an O_2-saturated 0.5 M H_2SO_4 solution and a N_2-purged 0.5 M H_2SO_4 solution; room temperature; sweep rate, 5 mVs^{-1}; rotation rate, 1,600 rpm. **c** Loss of electrochemical surface area (*ECSA*) of Pt/C and Pt/Fe_3O_4-CN_x catalysts with number of CV cycles in N_2-purged 0.5 M H_2SO_4 solution at room temperature (0–1.2 V versus RHE, sweep rate 100 mVs^{-1}). **d** Mass activity at 0.85 and 0.80 V (versus RHE) for Pt/Fe_3O_4-CN_x and Pt/C at the first and the 500 cycles

After 500 cycles, the stability of the catalytic activity was tested by immediately measuring the kinetic currents. It was found that the Pt/Fe_3O_4-CN_X exhibits a high mass activity of 5.2 (0.80 V versus RHE) and 8.7 (0.85 V versus RHE) times greater than those found for the Pt/C catalysts. The enhanced ORR activity of Pt nanoparticles deposited on the Fe_3O_4-CN_X may be attributed to the unique structure and properties of Fe_3O_4-CN_X, which can increase the electron supply from N element and the synergistic effect between Pt and Fe_3O_4-CN_X support when compared with conventional Vulcan XC-72R carbon support. Compared with Pt/C-CN_X, Pt/Fe_3O_4-CN_X presents better stability due to a strong interaction between Fe_3O_4-CN_X support and Pt nanoparticles, which can improve catalyst-support binding [38].

Conclusions

This study shows that Fe_3O_4, an alkaline oxide with low electrical conductivity, is a promising support material for Pt-based ORR electrocatalysts, after it was modified with CN_X. The *ECSA* values of Pt/Fe_3O_4-CN_X was found to be 21 % higher than that of conventional Pt/C. Compared with Pt nanoparticles deposited on carbon, the durability and activity of Pt nanoparticles are greatly enhanced on the Fe_3O_4-CN_X support. The electron from N element and the synergistic effect between Pt and Fe_3O_4-CN_X support result in a high activity towards ORR. Consequently from our study, the Fe_3O_4-CN_X appears to be a promising support material for DMFC electrocatalysts.

Acknowledgments We are really appreciated the National Natural Science Foundation of China (21163018), the National Science Foundation for Post-doctoral Scientists of China (20110490847, 2012 T50554), Guangdong Key Lab for Fuel Cell Technology, and the South African NRF (SUR 200806090021) for financially supporting this work.

References

1. Xiong LF, More KL, He T (2010) J Power Sources 195:2570– 2578
2. Zignani SC, Antolini E, Gonzalez ER (2008) J Power Sources 182:83–90
3. Kang YJ, Murray CB (2010) J Am Chem Soc 132:7568–7569
4. Huang SY, Ganesan P, Park S, Popov BN (2009) J Am Chem Soc 131:13898–13899
5. Gasteiger HA, Kocha SS, Sompalli B, Wagner FT (2005) Appl Catal, B 56:9–35
6. Franco AA, (2012) PEMFC degradation modeling and analysis (book chapter). In: Polymer electrolyte membrane and direct methanol fuel cell technology (PEMFCs and DMFCs) vol. 1: fundamentals and performance. C. Hartnig and C. Roth (eds.), Woodhead, Cambridge, UK
7. Franco AA (2008) Gerard M. J Electrochem Soc 155:B367–B384
8. Li WZ, Liang CH, Zhou WG, Qiu JS, Zhou ZH, Sun GQ, Xin Q (2003) J Phys Chem B 107:6292–6299
9. Miao ZL, Yu HM, Song W, Hao LX, Shao ZG, Shen Q, Hou JB, Yi BL (2010) Int J Hydrogen Energ 35:5552–5557
10. Travitsky N, Ripenbein T, Golodnitsky D, Rosenberg Y, Burshtein L, Peled E (2006) J Power Sources 161:782–789
11. Wang C, Daimon H, Sun SH (2009) Nano Letters 9:1493–1496
12. Kim DS (2010) Abo Zeid EF, Kim YT. Electrochim Acta 55:3628– 3633
13. Lopez N, Nørskov JK, Janssens TVW, Carlsson A, Puig-Molina A, Clausen BS, Grunwaldt JD (2004) J Catal 225:86–94
14. Suzuki S, Onodera T, Kawaji J, Mizukami T, Yamaga K (2012) Appl Catal A: General 427–428:92–97
15. Lee JM, Han SB, Kim JY, Lee YW, Ko AR, Roh B, Hwang I, Park KW (2010) Carbon 48:2290–2296
16. Chu YY, Wang ZB, Jiang ZZ, Gu DM, Yin GP (2011) Adv Mater 23:3100–3104
17. Tang YF, Allen BL, Kauffman DR, Star A (2009) J Am Chem Soc 131:13200–13201
18. Chen Z, Higgins D, Tao HS, Hsu RS, Chen ZW (2009) J Phys Chem C 113:21008–21013
19. Shao YY, Sui JH, Yin GP, Gao YZ (2008) Appl Catal B: Env 79:89–99
20. Gong KP, Du F, Xia ZH, Durstock ML, Dai LM (2009) Science 323:760–764
21. Xiao K, Liu YQ, Hu PA, Yu G, Sun YM, Zhu DB (2005) J Am Chem Soc 127:8614–8617
22. Zhou YK, Pasquarelli R, Holme T, Berry J, Ginleyc D, O'Hayre R (2009) J Mater Chem 19:7830–7838
23. Dommele SV, Jong KP, Bitter JH (2006) Chem Commun 42:4859– 4861
24. Zamudio AL, Rodríguez-Manzo JA, López-Urías F, Rodríguez-Gattorno G, Lupo F, Rühle M, Smith DJ, Terrones H, Díaz D, Terrones M (2006) Small 3:346–350
25. Liu YC, Wang CC (2005) J Phys Chem B 109:5779–5782
26. Chen YG, Wang JJ, Liu H, Norouzi Banis M, Li RY, Sun XL, Sham TK, Ye SY, Knights S (2011) J Phys Chem C 115:3769–3776
27. Jia NQ, Wang LG, Liu L, Zhou Q, Jiang ZY (2005) Electrochem Commun 7:349–354
28. Zhang H, Zhu G (2012) Appl Surf Sci 258:4952–4959
29. Padalia D, Johri UC, Zaidi MGH (2012) Physica B 407:838–843

30. Zhang DH, Liu ZQ, Han S, Li C, Lei B, Stewart MP, Tour JM, Zhou CW (2004) Nano Lett 4:2151–2155
31. Sun CL, Chen LC, Su MC, Hong LS, Chyan O, Hsu CY, Chen KH, Chang TF, Chang L (2005) Chem Mater 17:3749–3753
32. Su FB, Tian ZQ, Poh CK, Wang Z, Lim SH, Liu ZL, Lin JY (2010) Chem Mater 22:832–839
33. Barrado E, Montequi JI, Medina J, Pardo R, Prieto F (1998) J Electroanal Chem 441:227–235
34. Seger B, Kamat PV (2009) J Phys Chem C 113:7990–7995
35. Wang R, Zhang Z, Wang H, Lei Z (2009) Electrochem Commun 11:1089–1091
36. Chen ZW, Waje M, Li WZ, Yan YS (2007) Angew Chem 119:4138–4141
37. Wang W, Wang RF, Ji S, Feng HQ, Wang H, Lei ZQ (2010) J Power Sources 195:3498–3503
38. Saha MS, Li RY, Sun XL, Ye SY (2009) Electrochem Commun 11:438–441